Heikal et al., J Environ Hazard 2018, 1:1

Journal of Environmental Hazards

Research Article Open Access

Natural Radionuclides Levels and their Geochemical Characteristics of Abu Dabbab Albite Granite Mining Area, Central Nubian Shield of Egypt

Mohamed Th. S Heikal[1*], Mohamed Abd El Monsef[1], Saleh R Goma[2], Medhat M El Mansi[3] and Gulcan Top[4]

[1]*Department of Geology, Faculty of Science, Tanta University, Tanta 31527, Egypt*

[2]*SinoTharwa Drilling Company, Egypt*

[3]*Nuclear Materials Authority, Egypt*

[4]*Istanbul Technical University (ITU), Turkey & Szent Istvan University (SZIE), Hungary*

[*]**Corresponding author:** Mohamed Th. S Heikal, Department of Geology, Faculty of Science, Tanta University, Tanta 31527, Egypt, Tel: 2 01229457186; E-mail: mohamed.hekal1@science.tanta.edu.eg

Received date: November 09, 2018; **Accepted date:** December 20, 2018; **Published date:** December 24, 2018

Abstract

The present work addressed the natural radionuclides distribution and their geochemical characteristics for 21 albite granite samples, including surface, adit and subsurface core samples from Gebel Abu Dabbab rare metal-bearing albite granite (650-550 Ma). The measurements are provided by γ-ray spectroscopic analysis, including portable RS-230 model hand-detector and High Purity Germanium (HPGe) spectrometry. Chemical analysis using ICP-OES & ICP-MS have been carried out to determine the concentrations of major oxides and trace elements including U, Th (ppm) and ^{40}K % for the studied rocks. With respect to the field spectrometric measurements, the average radionuclide concentrations for point samples of eU, eTh (ppm) and K% were 10.36, 19.46 and 3.48 respectively. Gamma ray HPGe detector indicates that the average specific activities of ^{238}U, ^{232}Th and ^{40}K were 66.75, 29.97 and 641.68 Bq/kg for surface samples, respectively, 87.6, 57.3 and 329.4 Bq/kg for adit samples respectively, 87.3, 31.6 and 3.9 Bq/kg for subsurface core samples respectively. The average ratio is of $^{226}Ra/^{238}U<1$ indicating enrichment in ^{238}U due to its redistribution and remobilization. Regarding the chemical analysis for U, Th (ppm) and K%, the average concentrations were 6.90, 17.21 and 1.32 for surface samples as well as 8.33, 27.65 and 1.13 for adit samples, whereas the average concentrations of U, Th (ppm) and K% for the subsurface core samples were 4.85, 9.55 and 1.33 respectively. The radiometric, chemical data and the calculated P and D-factors of the studied radionuclides in Abu Dabbab rare metal-bearing albite granite confirmed that the redistribution of the radionuclides was formed later by hydrothermal Na-metasomatic albitization. All values of the radiation hazard indices in the studied samples of Abu Dabbab mining area are under the health hazard limits.

Keywords: Radionuclides; RS-230 spectrometer; HPGe gamma spectrometry; ICP-MS; OES chemical analysis; Albite granite mining area

Introduction

The natural radioactivity depends mainly on geological environments, in particular, special rock types and various processes that cause fractionations. It is largely known that alkali feldspar, zircon, apatite, allanite, sphene, xenotime and monazite, etc., represent the main sources of the light and heavy rare earth elements as well as radioactive concentrations, particularly, ^{238}U, ^{226}Ra, ^{232}Th and ^{40}K [1-6]. Also, the primordial ^{238}U is the most abundant isotope of U (99.27 %) and the initial member of the ^{238}U-decay chain with a long half-life time (4.4683 Ga) [7].

Uranium (U), Thorium (Th) and Potassium (K) are the main radionuclides that contribute to the natural terrestrial radioactivity. Thus higher radiation levels are associated with some felsic plutonic and volcanic rocks such as granites, syenites, rhyolites and dacites which are enriched with U and Th-bearing accessory minerals [8-15]. The measurement of the specific activities of the ^{238}U decay chain members and the correlation between them has been studied by numerous investigators in order to assess the presence of secular radioactive equilibrium [16-19].

One of the main processes governing the fractionation of U and Th-series nuclides is weathering process. It occurs frequently at shear zones where the fractionation causes enrichment of the radionuclides. This approach has been largely investigated by a lot of authors [20-25].

The present study aimed to discuss the distribution of the radionuclides and their geochemical characteristics; U, Th and K in surface and edit samples as well as some subsurface core samples at different depths. In addition, one of the main goals of the present study is to verify the relationship between natural radioactivity levels of U-Th-K and some major, trace and rare earth elements of the albite granite by the help of radioactivity and chemical data measurement comparison. Additionally, the ratio-diagrams of U, Th and K% concentrations are used to delineate the redistribution processes of the studied radioelements.

Geology

The study area is located at the northwestern of Marsa Alam town, central Nubian Shield of Egypt (Figure 1). The Gebel Abu Dabbab rare metals-bearing albite granite represents one of Late Pan-African alkaline plutons of granitic rocks (650-570 Ma, [26,27]. It constitutes a promising mining profit of cassiterite ore and enriched in rare-metals (Ta and Nb) in the form of disseminated grains and numerous mineralized quartz veins cross cutting hosting albite granite. Therefore

Citation: Heikal MTS, Monsef MA, Goma SR, Mansi M, Top G (2018) Natural Radionuclides Levels and their Geochemical Characteristics of Abu Dabbab Albite Granite Mining Area, Central Nubian Shield of Egypt. J Environ Hazard 1: 108.

it has attracted many investigators for being most important rare-metal mining areas in the Eastern Desert [28-32].

The Abu Dabbab mapped area covers some 2 km^2 (Figure 1). It includes two main rock successions; ophiolitic mélange (the oldest) and rare metal-bearing albite granite (the youngest). The ophiolitic mélange (1.6 km^2) comprises excotic blocks of serpentinites, mafic metavolcanics, metasediments and their assortment of amphibolites and hornfelses respectively , rare metal-bearing albite granite (0.4 km^2) constitute Gebel Abu Dabbab itself, representing the main target of the present work. It comprises albite granite of variable sizes and textures forming a stock-like intrusion of ellipsoidal-shaped with offshoots in the form of the elephant's long nose (about 100 m in length, Figure 1) lie toward northwest of the stock.

Points	K (%)	eU (ppm)	eTh (ppm)	eTh/eU	eTh/3.5	eTh/K	Remarks
P1	4.5	19.5	42	2.15	12	9.33 x10^{-4}	Sheared granite-left side of adit #3
P2	3.3	13	18	1.38	5.14	5.45 x10^{-4}	At the entrance ofadit #3(Contact)
P3	3.7	9.9	24	2.42	6.86	6.49 x10^{-4}	Inside of adit #3 (Quarried)
P4	3.5	19	30	1.58	8.57	8.57 x10^{-4}	Sheared granite-right side (Away) of adit #3
P5	4	20	35	1.75	10	8.75 x10^{-4}	Sheared granite-right side (Away) of adit #3
P6	4	13	29	2.23	8.29	7.25 x10^{-4}	Sheared granite
P7	3.4	6.6	13.3	2.02	3.8	3.91 x10^{-4}	Sheared granite
P8	2.4	10.5	8.6	0.82	2.46	3.58 x10^{-4}	Sheared granite
P9	2.7	7.7	9.6	1.25	2.74	3.56 x10^{-4}	Sheared granite
P10	3.1	5.1	11.5	2.25	3.29	3.71 x10^{-4}	Sheared granite
P11	3.1	9.2	23	2.5	6.57	7.42 x10^{-4}	Sheared granite
P12	3.8	6.9	18	2.61	5.14	4.74 x10^{-4}	Sheared granite
P13	3.1	6.7	13.8	2.06	3.94	4.45 x10^{-4}	Sheared granite
P14	4.6	9.8	19.7	2.01	5.63	4.28 x10^{-4}	Sheared granite
P15	4	10.7	12.3	1.15	3.51	3.08 x10^{-4}	Sheared granite
P16	4	12.5	21	1.68	6	5.25 x10^{-4}	Sheared granite
P17	4.8	12.5	19.7	1.58	5.63	4.10 x10^{-4}	Sheared granite
P18	3.1	7.6	13.5	1.78	3.86	4.35 x10^{-4}	Sheared granite
P19	4	12.5	20	1.6	5.71	5.00 x10^{-4}	Sheared granite
P20	5.6	7.5	13	1.73	3.71	2.32 x10^{-4}	Near amazonite vein
P21	3	10	15	1.5	4.29	5.00 x10^{-4}	Near amazonite vein

Table 1: Calculated relative radionuclide concentrations (K, eU and eTh) provided by RS-230 spectrometer for Abu Dabbab albite granite.

The present rare metal-bearing albite granite stock intrudes into an ophiolitic mélange with knife-sharp contact. Its contact with ophiolitic country rocks dips away from the granite with attitudes: 220º/70º SE and 300º/65º NE.

In addition,the chilled margins range from 15 cm to 30 cm wide near the contact between albite granite and the ophiolitic metavolcanics. There is a stock of scheider marginal pegmatite at the southwestern contact (Figure 2). Regarding, this pegmatite, it is currently under focous by funded project from the Nuclear Materials Authority of Egypt.

All the present rock units are cross cut by faults and shear zones. Almost rock successions are dissected by quartz-bearing cassiterite (Figure 3a) and amazonite veins as well as mafic and felsic dykes.

On the basis of the structural implications of the Abu Dabbab rare-metal albite granite and its country ophiolitic mélange are bounded and intersected by N-S, NE and NW shear zones that are likely linked with the Najd Fault System (Figure 1) [33]. At the southern end on both ophiolitic mélange and albite granite, the shear zones and quartz tension veins as well as gresienization are well reported. These shears continue further north and are confined to the contact zones in the marginal parts of the albite granite outcrop. The main components of the shear zone are highly deformed granite sheets that tend to be

Citation: Heikal MTS, Monsef MA, Goma SR, Mansi M, Top G (2018) Natural Radionuclides Levels and their Geochemical Characteristics of Abu Dabbab Albite Granite Mining Area, Central Nubian Shield of Egypt. J Environ Hazard 1: 108.

mylonitic fashion (Figure 3b). Field evidences of slicken-sided striations suggest that shear deformation was active throughout the evolution of the Abu Dabbab albite granite.

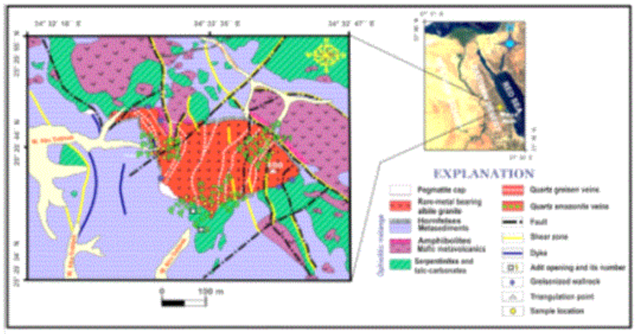

Figure 1: Geological map of Abu Dabbab rare-metal bearing albite granite area (after Heikal et al., 2018) The yellow solid circles represent the locations of the points sample measured by RS-230 spectrometer. Code samples refer to Table 1.

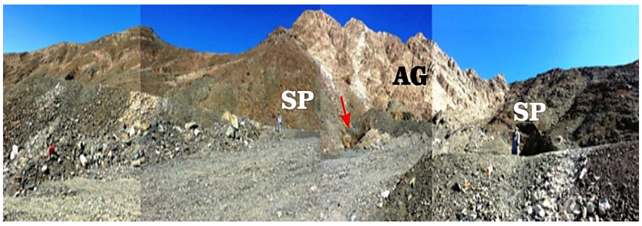

Figure 2: Panoramic view of Abu Dabbab albite granites (AG) at the southern end which intrudes ophiolitic serpentinites (SP) on both sides. Note adit # 1 (arrows) relevant to mining profit.

Analytical Techniques

Portable gamma-ray spectrometer

During the field work the radiometric survey performed by RS- 230 BGO Super-Spec model portable radiation detector with 95% relative efficiency (Figures 3c,3d), handheld unit spectrometer survey meter with high accuracy. This detector is full assay capability with data on K %, eU (ppm) and eTh (ppm), no radioactive sources required for proper operation. The RS-230 detector was manufactured by an independent private company (Radiation Solutions, Inc., 386 Watline Ave, Mississauga, Ontario, Canada, L4Z 1X2).The term 'equivalent' or its abbreviation 'e' is used to indicate that the equilibrium is assumed between the radioactive daughter isotopes monitored by the spectrometer, and their respective parent isotope.

A joint Egyptian-Soviet team had been established on Abu Dabbab albite granite under cooperative contract (1975). A total of 17 diamond drill holes, three adits, one crosscut, numerous trenches and surface sampling were completed during this period. Bulk sampling and processing tests were carried out in 1973-1974 and a "techno-economic feasibility report "1" was completed in 1975.

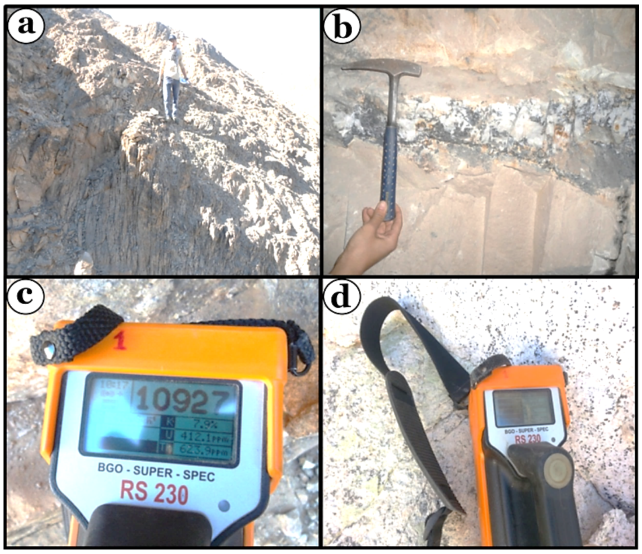

Figure 3: **a.** Highly sheared albite granite, giving rise to mylonitic fashion. It is located along master shear, **b.** pegmatitic quartz vein-bearing mineral-ization invades albite granite inside adit, **c.** Screen photo of RS-230, **d.** A point sample measured by RS-230 spectrometer for massive albite granite.

In the present study, the total gamma measurements for 21 point samples, including surface and adit of the studied Abu Dabbab albite granite were taken by the RS-230 model handheld detector (Figures 1 and 3c,3d, Table 1). The samples carried out parallel and 10-15 m apart from a grid pattern taken as reference (Figures 1 and 3). The space between measurement stations was smaller (2-5 meters) at higher strain shear zones. They were considered to investigate their natural radioactivity due to ^{238}U, ^{232}Th and ^{40}K radionuclides. The calibration procedure of the detector establishes the proportionality between the measured counts and the ground concentrations of U, Th and %K. So as to enable the qualitative determination of the radioelement composition in the surface rocks and soil samples. The instruments are calibrated using international standards that were developed by the Geological Survey of Canada (GSC) traceable by IAEA. Before field measurements, the RS-230 spectrometer was calibrated on concrete pads containing known concentrations of U, Th and K. The measurements were based on the detection of γ-radiation emission in the decay of ^{214}Bi (^{238}U series) at 1.76 MeV, ^{208}Tl (^{232}Th series) at 2.41 MeV, and the primary decay of potassium ^{40}K (1.46 MeV) measured directly. U and Th activity determinations were based on the assumption that the daughter nuclides are in equilibrium with the parent nuclides. Consequently, the deduced amounts of uranium and thorium are equivalent to what would be in equilibrium with the measured radioactivity of the bismuth or thallium isotopes. Therefore the term 'equivalent' or its abbreviation 'e' is used to indicate that the equilibrium is assumed between the radioactive daughter isotopes monitored by the spectrometer, and their respective parent isotope.

Sample preparation

Twenty-one surface, adit and subsurface core samples (200-230 m in depth, Tantalum-Egypt Company) were carefully collected from Abu Dabbab rare metal-bearing albite granite represent the entire Ta-Nb-Sn mining area (Figure 1). Almost samples were enriched with accessory minerals such as zircon, allanite and apatite. The samples, each about 250 gr were packaged in well labeled polyethylene bags, and transported to the Nuclear and Radiological Regulatory Authority, Cairo for analysis in the radiation protection laboratory. The samples were air-dried at ambient temperature at 100°C for 72 hours. The dried samples were pulverized, sieved (200 mesh), and thoroughly homogenized. 185 ± 10 gr of the homogenized samples were carefully packed into well-labeled Marinelli beakers and properly sealed to prevent the escape of radon. The sealed samples were stored for about four weeks to attain radiological (secular) equilibrium where the decay rates of the daughter nuclides and their respective parents become equal [34,35].

Gamma-ray spectroscopy

Activity measurements for 21 samples (Table 2) have been performed by the Radiation Protection Laboratory using a vertical HPGe detector of relative efficiency 40% and full width at half maximum (FWHM) of 2.0 keV for ^{60}Co gamma energy line at 1332 keV. The detector was operated by Canberra Genie 2000 software for gamma acquisition and analysis. The Hyper Purity Germanium (HPGe) detector was containing 4 inches thick low background lead shield for germanium detectors in the free standing lead-originated castle providing a low background environment to shield the detector from lead fluorescent X-rays and bremsstrahlung, the lead was lined with 1 mm tin and 1.6 mm copper metals.

The specific activity calculations of ^{238}U and ^{232}Th were obtained indirectly from the gamma rays emitted by their progenies which were in secular equilibrium with them. The determination of ^{226}Ra activity was based upon the detection of 351.9 keV gamma rays emitted from ^{214}Pb, 609, 1120, 1764 keV from ^{214}Bi and 295 keV from ^{214}Pb. The determination of ^{232}Th activity, was found by the detection of 238.6 keV gamma rays from ^{212}Pb, 911.2 and 969 keV from ^{228}Ac, 583.34 keV gamma rays from ^{208}Tl, while ^{40}K activity concentration was determined from the 1460.7 keV gamma line. After background corrections, the net area under each photo peak was used to calculate the activity concentration of each radionuclide in samples.

Chemical analysis

Representative (22) fresh samples of rare metals-bearing albite granites were selected for geochemical analyses of some major, trace elements, REEs and U-Th concentrations (Tables 3 and 4). All samples selected cover the areal distribution of the studied granitic stock (Figure 1). They were crushed and powdered using special agate mortar to avoid trace elements contamination and were prepared for complete chemical analysis using fused tablets with $LiBO_2$ and HNO_3 dissolution in the laboratory of ALS CHEMEX, Ireland. Samples were analyzed by ICP-OES for ME-ICP06 and ME-4ACD81 by two different Agilent 725 ICP-OES (Serial numbers IP0807M048 and AU12370004) using a Niagara Switching valve from Glass expansion and an AIM3600 auto-sampler from AIM lab. Voltage for the ICP-OES was 220 V. They were also analyzed by ICP-MS for ME-MS81 in our Agilent 7700 ICP-MS (Serial number JP11401316) using also a Niagara Switching valve and an AIM3600 auto sampler from AIM lab. for the ICP-MS. In summary, the Optical Emission Spectrometry (ICP-OES) technique has been used for the major oxides, while Mass Spectrometry (ICP-MS) was applied for trace elements and REEs, including U and Th.

Petrographic inspection

All thin sections have been studied under transmitted polarizing research microscope model OPTIKA-500, ITALY to identify the main rock type and its mineralogical composition. Petrographically, the main rock type in Gebel Abu Dabbab is albite granite which is relevant to alkali feldspar granite.

Microscopically, they were composed of albite (An 6-10), microcline and micas (Figure 4a). Accessories include zircon, apatite, allanite and opaques (Figures 4a,4b). Secondary products were kaolinite, sericite and chlorite. Snowball, seriate and poikilitic textures as well as shearing were well pronounced. Albite (An 6-10) was the main mineral constituent in these rocks (50% by total volume percent). It occurred either as minute euhedral laths up to 0.12 mm long or large euhedral to subhedral prismatic crystals up to 1.2 mm across. In addition, numerous albite crystals were found as inclusions within quartz and microcline, proved that albite was the first crystallized mineral. Quartz (25% by total volume) occurred in two generations; the first one formed subhedral to anhedral chessboard crystals up to 2 mm across. They contained poikilitic inclusions of albite laths and muscovite flakes as well as they embraced the characteristic texture, where albite laths arranged along the growth zone of quartz giving rise to snowball texture. The second generation formed fine anhedral crystals filling the interspaces among the mineral constituents Potash feldspar (15 % by total volume) was represented by microcline that formed euhedral to anhedral crystals up to 1.6 mm across. Gridiron twinning is well recognized and some crystals tend to be replaced partially by muscovite. Micas (10% by total volume) were represented by muscovite. It formed subhedral and anhedral flakes and patches up to 2 mm across, replacing alkali feldspar as a result of sub-solidus metasomatism leading to greisenization process. Moreover, the major gain of albite and loss of microcline in many slides is due to sodic metasomatism that occurred in these rocks. On the other hand, shearing was well pronounced throughout the mineral constituents giving rise to strain shadows, cracking, bending and twisting features. Accessories (less than 2% by total volume) included zircon, allanite and apatite (Figures 4a-4c). Also opaques included Ta-Nb-Sn -bearing minerals; cassiterite and columbite-tantalite association (Figure 4d) and iron-manganese oxides (dendritic clusters throughout the rocks and films along grain boundaries). They were sporadically scattered on the rock, but in some samples were clustered aggregates. Sericite, kaolinite and chlorite occurred as alteration products of albite, alkali feldspar and micas respectively. There were no any relics of uranium and/or thorium minerals throughout the rocks.

Results and Discussion

Distribution of radionuclides (^{238}U, ^{226}Ra, ^{232}Th and ^{40}K)

Radionuclides (^{238}U, ^{226}Ra, ^{232}Th and ^{40}K) distribution throughout the surface, adit and subsurface core samples were determined by various techniques.

For radioactivity measurements portable gamma ray RS-230, detector and HPGe gamma ray spectroscopy whereas radioelements (U, Th and K) were determined by chemical analysis using (ICP-MS & OES).

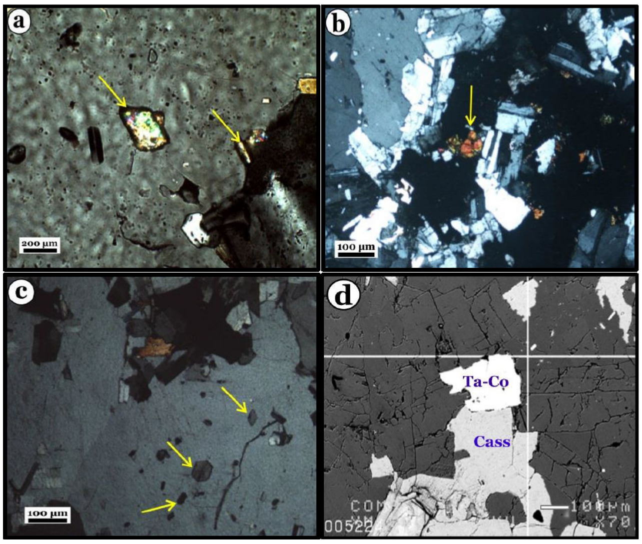

Figure 4: Photomicrographs of albite granite between crossed polars, **a.** A bold crystals of zircon (arrows) as inclusions within quartz host, **b.** An allanite crystal (arrow) as disseminated grains among the main mineral constituents (albite, microcline and quartz), **c.** A minute six-sided prismatic crystals of apatite (arrows) within large crystal of quartz, **d:** Backscattered electron photomicrograph showing anhedral cassiterite crystal (Cass) of brownish grey color adjacent to columbite-tantalite association (Co-Ta) of white with brownish tint.

Regarding *in situ* point gamma-ray measurements definitely appeared to be a useful and sensitive method for obtaining actual information on radionuclides in the environment, and its use for the quantitative and fast assessment of uranium, thorium and potassium concentrations offers a number of advantages when compared with the conventional laboratory analysis. In fact, this method provides immediate results which are representative for a relatively large volume of rock (some order of magnitude larger than that of a conventional hand specimen). Moreover, field γ-ray radiometric surveying facilities are good for the rapid mapping of geological formations, especially in rough terrain and are appropriate for both measurements and detailed mapping of radioelement concentrations.

Regarding the field radiometric measurements of surface and adit samples (Table 1), the albite granites were characterized by radionuclides concentrations ranging from 5.1 to 20 ppm with an average 10.36 ppm for eU, from 8.6 to 42 ppm with an average 19.46 ppm for eTh and from 3.1 to 4.8% with an average of 3.48% for K (Table 1 and Figure 5). It was noticed that the higher contents of eU and eTh were closely related to sheared albite granites nearby or inside the adits, whereas massive albite granite gave rise to low values of eU and eTh (Table 1). On the other hand, the specific activities of the studied surface albite granite samples (Table 2) ranged from 48.05 to 94.68 Bq/kg with an average of 66.75 Bq/kg for U, from 29 to 61.52 Bq/kg with an average 46.2 Bq/kg for Ra, from 9.51 to 45.10 Bq/kg with an average 20.1 Bq/kg for Th and from 74.25 to 1051.62 Bq/kg for K. While, the adit albite granite samples (Table 2 and Figure 5) uranium specific activities were varied between 33.43-206.47 Bq/kg with an average 87.6 Bq/kg, and finally for potassium specific activities were varied between 66.81-659.35 Bq/kg with an average value 329.4 Bq/kg. With respect to radioactivity concentration of core samples (Table 2 and Figure 5), uranium ranged from 66.28 to 108.23 Bq/kg with an average 87.3 Bq/kg, for radium ranged from 46.08 to 54.17 Bq/kg with an average 50.1 Bq/kg, thorium ranged from 19.68 to 43.47 Bq/kg with an average 31.6 Bq/kg and K ranged from 728.39 to 939.42 Bq/kg with an average 833.9 Bq/kg. Consequently, the given results (Table 2 and Figure 5) of the eU, eTh, and K specific activities measured from the field were about twice higher than those found samples measured by laboratory HPGe gamma ray spectroscopy. This attributed to huge background radiation in the studied field area (Figure 1), which arising from primordial radionuclides (uranium, thorium, their decay products and potassium), whereas the measured samples in the laboratory represent a small-size ones; about 250 gr for each sample [36].

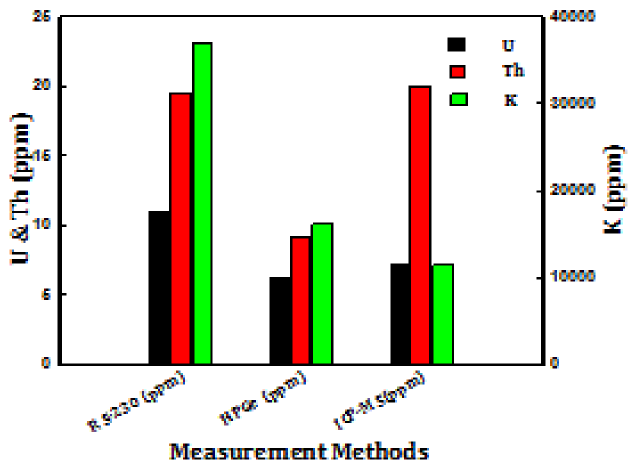

Figure 5: Tentative comparison with an average U, Th and K concentrations of the Abu Dabbab albite granite by the help of various radiometric methods and chemical analysis.

It is clear from Table 2 that almost specific activities of ^{226}Ra,^{238}U, Th^{232} and ^{40}K radionuclides had values below the average permissible limits recommended by [37,38] (32 Bq kg^{-1} for ^{226}Ra, 33 Bq Kg^{-1} for ^{238}U, 45 Bq kg^{-1} for Th and 412 Bq kg^{-1} for ^{40}K). Some exceptional concentration values are reported of the studied radionuclides relevant to adit samples (Table 2). In terms of ^{40}K, the specific activities of surface, adit and subsurface core samples were under investigation and had an average as 588.33 Bq/ kg, which is about 7 times higher than ^{238}U, 12 times higher than ^{226}Ra and 10 times higher than ^{232}Th (Table 2). This implies that the largest contribution to the total specific activity refers to ^{40}K in the studied rocks, in which the modal composition of potash feldspar minerals in the studied albite granite up to 22% by volume percent. In addition, the obtained results showed that the Raeq of all samples had values (Table 2) less than the permissible maximum value which was also verified by [1], who concluded that the hazard indices of Abu Dabbab albite granite are within the safe dosage limits specified in international standards (UNSCEAR 2008 and ICRP 2014).

Regarding the chemical analysis used by ICP-MS of U, Th (ppm) and CP-OES of K% for 22 samples (Table 3 and Figure 5), the elemental concentrations for U in surface samples ranged from 4.31 to 14.15 ppm with an average 5.84 ppm, for Th ranged from 3.45 to 76.7 ppm with an average 14.6 ppm, and for K2O% ranged from 2.04 to

4.97 % with an average value 3.61 %. U ranged from 2.56 to 16 ppm with an average 8.33 ppm, Th ranged from 4.29 to 86.4 ppm with an average 27.66, and K_2O % ranged from 0.27 to 3.8 % with an average 2.28% in adit samples. The concentrations of U, Th, K_2O % of core samples ranged from 3.48 to 7.49 ppm with an average 4.85 ppm, and 4.22 to 20.9 ppm with an average value 9.55 ppm, and 2.99 to 3.72 % with an average 3.24 %, respectively.

When we throw a spotlight on the mentioned data above, concerning, the concentrations tend to be equal for all exposure types with exceptional case of adit samples and core subsurface samples. The adit samples represent the highest radioactivity concentrations on both uranium and thorium and they have the considerable concentration values of K_2O %, where core samples had higher concentrations of K_2O % and lower concentrations of U & Th if compared with surface and adit samples. This attributed that the adit samples emit a lot of radon-indoor gas associated with mineralized pegmatitic quartz veins occurrences (Figure 3b) due to the highest concentrations of their U & Th contents. In literatures, the radioactive daughters ^{222}Rn, ^{220}Rn and ^{219}Rn are being gaseous and thus can move away from their respective source materials (^{238}U, ^{235}U and ^{232}Th), through the process of forced and/or natural migration [19,39] and they may also be carried away owing to the convectional flow of fluids in the earth's crust. In general, the radon enrichment appears to be relevant with the locations of the faults, joint and tension quartz veins [39,40].

Sample No.	Sample type	Radium activity concentration ARa (Bq/kg)	Uranium activity concentration AU(Bq/kg)	Thorium activity concentration ATh (Bq/kg)	Potassium activity concentratn AK (Bq/kg)	ATh/AK	ATh/3.5	ATh/AU
AD1	Surface Samples		50.59	17.25	74.25	0.23	4.9	0.34
AD3			74.87	45.1	354.47	0.13	12.9	0.6
AD4			58.13	9.51	593.2	0.02	2.7	0.16
AD5			76.09	14.53	889.32	0.02	4.2	0.19
AD24			94.68	14.7	1051.62	0.01	4.2	0.16
AD28			68.62	15.13	664.74	0.02	4.3	0.22
AD30			88.15	26.92	417.06	0.06	7.7	0.31
AD31			47.7	9.47	675.2	0.01	2.7	0.2
AD32			60.64	17.96	658.34	0.03	5.1	0.3
AD33			48.05	29.97	641.68	0.05	8.6	0.62
Mean ± SD			66.75 ± 16.6	20.1 ± 11.01	601.9 ± 225	0.03	5.7	0.3
AD8	Adit Samples		100.09	118.42	609.49	0.19	33.8	1.18
AD13			152.3	115.39	66.81	1.73	33	0.76
AD15			32.72	16.45	300.16	0.05	4.7	0.5
AD16			206.47	198.07	408.89	0.48	56.6	0.96
AD20			74.81	20.56	145.22	0.14	5.9	0.27
AD22			56.91	8.59	569	0.02	2.5	0.15
AD23			33.43	14.75	110.22	0.13	4.2	0.44
AD25			72.18	12.42	659.35	0.02	3.5	0.17
AD26			59.16	10.8	95.36	0.11	3.1	0.18
Mean ± SD			87.6 ± 57.6	57.3 ± 69.2	329.4 ± 182.3	0.17	16.4	0.65
CS-5 200 m in depth	Core Samples		66.28	43.47	728.39	0.06	12.4	0.66
CS-6 230 m in depth			108.23	19.68	939.42	0.02	5.6	0.18

Mean ± SD			87.3 ± 29.7	31.6 ± 16.8	833.9 ± 149.2	0.04	9	0.36

Table 2: Specific activities of ARa, AU, ATh, and AK of the studied samples.

Sample Code	Sample type	Na2O (%)	K2O (%)	A/CNK	K (ppm)	K (%)	U (ppm)	Th (ppm)	U/Th	Th/U
AD1	Surface Samples	6.2	2.56	1.12	10621	1.1	4.31	6.64	0.65	1.54
AD3		6.7	2.05	1.08	8505	0.9	6.99	18.5	0.38	2.65
AD4		6.23	2.3	1.1	9543	1	6.33	17.2	0.37	2.72
AD5		4.93	4.97	1.14	20620	2.1	7.66	9.05	0.85	1.18
AD9		6.62	2.34	1.01	9709	1	14.15	76.7	0.18	5.42
AD11		7.12	2.04	1.09	8463	0.8	7.37	12.9	0.57	1.75
AD28		5.3	3.58	1.1	14853	1.5	5.28	6.83	0.77	1.29
AD29		5.61	3.68	1.1	15268	1.5	5.31	17.6	0.3	3.31
AD30		6.79	2.28	1.04	9460	0.9	6.17	8.49	0.73	1.38
AD31		5.4	3.81	1.07	15808	1.6	4.57	3.45	1.32	0.75
AD34		5.67	2.92	1.03	12115	1.2	7.74	12.45	0.62	1.61
AD13	Adit Samples	6.74	0.27	1.06	1120	0.1	12.45	52	0.24	4.18
AD10		10.5	0.6	1	2489	0.2	8.9	34	0.26	3.82
AD15		5.19	2.72	1.35	11285	1.1	2.65	9.01	0.29	3.4
AD16		6.72	2.28	1.03	9460	0.9	16	86.4	0.19	5.4
AD17		6.06	3.02	1.12	12530	1.3	10.6	24.6	0.43	2.32
AD19		5.6	3.14	1.11	13028	1.3	6.58	5.17	1.27	0.79
AD22		4.91	2.46	1.17	10206	1	4.33	5.77	0.75	1.33
AD25		5.32	3.8	1.08	15766	1.6	5.15	4.29	1.2	0.83
CS-1	Core Samples	5.02	2.99	1.21	12405	1.2	3.57	3.52	1.01	0.99
CS-4		6.08	3.72	1.07	15434	1.5	7.49	20.9	0.36	2.79
CS-6		5.07	3.03	1.19	12571	1.3	3.48	4.22	0.82	1.21

Table 3: Chemical analyis of some major elements, U, Th and K concentrations and their chemical ratios of the studied samples.

In respect of the high concentration of K_2O % in the studied core samples, this is due to inactive weathering and alteration processes leading to the presence of unharmed fresh alkali feldspar minerals.

Radiometric data interpretations

We are going to donate and delineate the most common radiometric data relationships among specific activities of ^{238}U, ^{232}Th and ^{40}K (Tables 1 and 2) using variation diagrams for the resultant data.

Radiometric data using RS-230 handheld and HPGe gamma spectrometer

A total of 21 point samples of albite granite measured by portable RS-230 for the elemental concentrations of eU, eTh (ppm) and K% (Table 1). Almost sample locations were carefully chosen along shear zones which were measured and determined by HPGe detector and ICP-MS and OES techniques respectively were very close to the point samples. The following relationships among these elemental ratios (Figure 6) for the field samples are given below. The relation and concept of eU- eTh/3 [41] is related with the increasing of the initial Th/U ratio in the studied albite granite which occurred due to the immobility of thorium relative to uranium. This is well shown in the (eU-eTh/3.5) (Table 1) giving positive values for the U-enriched zones or negative values in the case of U- depleted zones according to the subtraction of the original magmatic uranium (eTh/3.5) from the measured uranium (eU). It is very helpful in defining the trends of uranium migration [41]. Figure 6a reveals positive correlation indicating U-Th enriched zones.

The K-eTh plot (Figure 6b) is widely used for the recognition of alteration products of sodic plagioclase (albite) and potash feldspar (microcline) [42]. So, If eTh/K $\geq 2 \times 10^{-4}$, the rock is relevant to thorium rich, and if eTh/K $\leq 1 \times 10^{-4}$, the rock is being potassium rich [43]. In the present study, the albite granite is pertaining to (Figure 6b) thorium rich rocks (Table 1).

From Table 1, the average value of eTh/eU ratio for the studied rocks is 1.88. This value is lower than the Clark value (3.5) which indicates that the radioelements in these rocks have been significantly fractionated or involved during hydrothermal metasomatism [44]. In addition, the positive relationship between eTh-eU; Figure 6c indicates an early magmatic process in the studied albite granite.

The plots of eTh /eU *vs* eTh diagram exhibits positive correlation (Figure 6d) confirming magmatic process for the studied albite granite, as verified by [45].

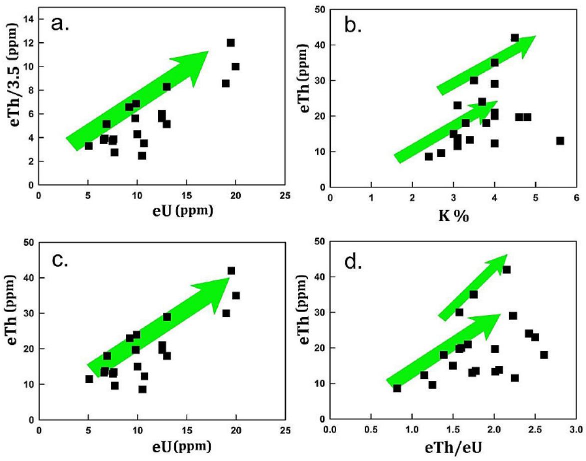

Figure 6: (A-D) Variation diagrams of eU, eTh (ppm) and K% relevant to portable γ-ray RS-230 spectrometer for point samples.

Radiometric data obtained by HPGe detector

A total number of 21 samples from Abu Dabbab albite granite were subjected to radiometric analysis for the determination of ^{238}U, ^{226}Ra, ^{232}Th and ^{40}K activity concentrations in Bq/kg (Table 2) and their ppm equivalents calculated.

Regarding eU *vs* eTh/3.5 diagram (Figure 7a), the plots display slight positive correlation indicating U-enriched zone for the studied samples.

In respect of eTh vs. eU diagram (Figure 7b), the plots show a slight positive relation giving rise to post magmatic process has been elucidated. The mean values of Th/U are 0.30, 0.65 and 0.36 for the surface, adit and core samples, respectively (Table 2) indicating magmatic process as mentioned by [44].

With respect to K *vs.* eTh diagram (Figure 7c); the irregular trends are relevant to the plots. The mean values of Th/K ranged from 0.04 to 0.17 (Table 2) indicating that the rocks are being thorium-rich [43].

The plots of eTh/eU *vs.* eTh (Figure 7d) reveal a slight positive correlation indicating magmatic processes.

Regarding eU *vs.* eRa diagram (Figure 7e); the plots indicate a strong positive correlation. This is attributed to that ^{226}R a is closely related to daughters of ^{238}U.

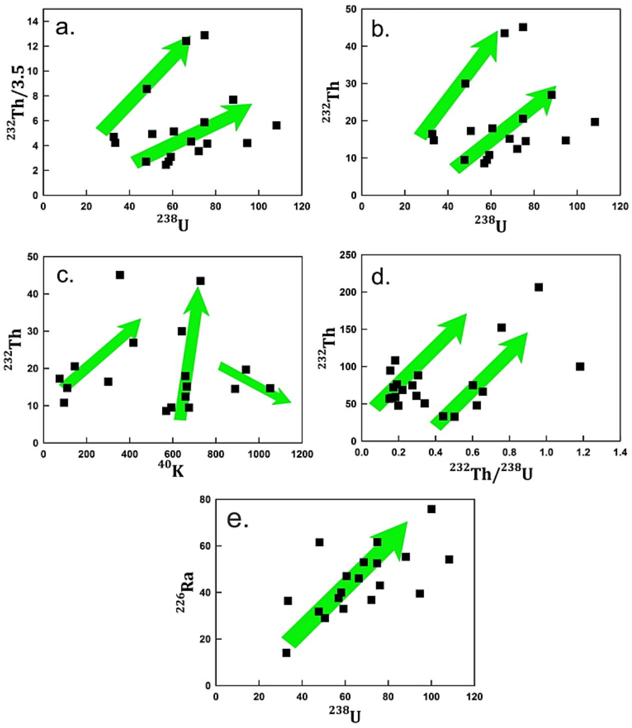

Figure 7: (a-e) Variation diagrams among ^{238}U, Ra^{226}, ^{232}Th and ^{40}K (ppm) relevant to γ-ray HPGe spectroscopic measurements for the studied samples.

Geochemical characteristics of U, Th and K

On the basis of chemical analysis of the studied radioactive elements and other selected elements (Tables 3 and 4), U and Th concentrations in the studied albite granites ranged from 3.48 to 16 and from 4.22 to 86.4 ppm, with an average 7.13 and 19.99 ppm respectively (Table 3). They have high contents, if compared with average U and Th contents of the upper continental crust composition (2.7 ppm for U and 10.5 ppm for Th).The significant feature of the studied samples reveals that the concentration of Th is higher than U . In addition, K% in the present rocks varied from 0.2 to 1.6 with an average of 1.13 % (Table 3) which equals to 354 Bq/kg (Table 2).

We are going to discuss the given chemical data of U, Th and K concentrations together with some selected major, trace and rare earth elements in the studied albite granite (Tables 3 and 4) for delineating the geochemical characteristics and origin of the radioactive elements herein.

Variation diagrams of U, Th and K

On the basis of the given chemical data of U, Th and K concentrations (ppm) for the studied albite granite (Table 3 and Figures 8a,8b), it is noted that the increasing trend of U concentrations meets increasing Th (Figure 8a) reflecting magmatic signature. This is the usual case in felsic igneous rocks. On the other hand, the relation U *vs.* (U-Th/3.5) (Figure 8b) reveals uranium enrichment [45] for the studied albite granite samples.

Alumina saturation index in relation with U, Th and K

According to the plotting for the molecular ratios of Al_2O_3/(CaO + Na_2O + K_2O) symbolic as A/CNK *vs* U, Th and K (Figures 9a, 9b and Table 3), the slight negative correlation is apparently obvious. This suggests that the studied samples with lower A/CNK values have the highest concentrations of U and Th and K, consistent with published work [19].

Correlations with major, trace and rare earth elements

The studied radionuclides measured by using ICP-MS method have been correlated with some selected major (ICP-OES) and trace elements as well as REEs (ICP-MS) (Tables 3 and 4 and Figures 10 and 15). They are characterized by high contents of Na_2O ranged from 4.91 to 10.5 wt.%, low to moderate contents of K_2O up to 5 wt.%, whereas as CaO and Fe2O3 have low contents (Table 3).

Regarding Na_2O *vs* U & Th (Figures 10a, 10b), strong positive correlations are well obvious, whereas the moderate negative correlation between K_2O and U & Th (Figures 10c, 10d). This suggests that the increasing trend between Na_2O and U & Th refer to Na-metasomatic albitization (albite is about 45% model composition) do occur and decreasing trends of K_2O meet high values of U & Th.

Sample	Rb	Nb	Ta	Sn	Y	Zr	Zr/K%	Zr/U	Zr/Th	Hf	LREEs	HREEs	ΣREEs
Code	(ppm)	(ppm)	(ppm)	(ppm)	(ppm)	(ppm)				(ppm)	(ppm)	(ppm)	(ppm)
AD1	402	53.7	120.5	1010	1.8	40	36.36	9.28	6.02	25.4	14.02	11.97	25.99
AD3	318	86	254	696	1.6	64	71.11	9.16	3.46	41.1	15.61	12.6	28.21
AD4	426	95.4	299	3900	2	31	31	4.9	1.8	18.7	15.4	12.07	27.47
AD5	935	85.7	265	631	2	61	29.05	7.96	6.74	33.4	9.22	12.44	21.66
AD9	311	82.6	267	3460	1.5	87	87	6.15	1.13	56.7	13.54	13.69	27.23
AD11	333	105	238	1300	2	80	100	10.85	6.2	55.7	9.35	13.75	23.1
AD28	698	66.5	162.5	801	0.7	33	22	6.25	4.83	17.9	15.22	6.62	21.84
AD29	643	76.5	159	654	1	33	22	6.21	1.88	16.8	20.26	11.96	32.22
AD30	448	26.9	189	1880	1.4	65	72.22	10.53	7.66	50.4	8.96	10.37	19.33
AD31	741	87	229	1360	0.7	37	23.13	8.1	10.72	20.1	14.33	6.3	20.63
AD34	469	35	183.5	2260	1.1	90	75	11.63	7.23	64.7	13.05	8.02	21.07
AD10	95	93.7	171	186	1.1	72	720	5.78	1.38	45.5	11.61	11.55	23.16
AD13	46	165	314	481	1.6	101	505	11.35	2.97	57.2	8.57	16.15	24.72
AD15	1050	23	130.5	3090	1	31	28.18	11.7	3.44	18.8	16.86	7.55	24.41
AD16	324	139	300	317	0.6	93	103.33	5.81	1.08	68.9	13.13	11.23	24.36
AD17	626	87.4	473	2200	3.3	101	77.69	9.53	4.11	70.2	14.71	18.35	33.06
AD19	580	66.5	167	707	1	47	36.15	7.14	9.09	26.9	14.88	9.35	24.23
AD22	469	60.4	167.5	963	0.9	33	33	7.62	5.72	22.1	8.75	6.09	14.84
AD25	649	66.4	201	1055	1.1	39	24.38	7.57	9.09	23.8	13.69	8.13	21.82
CS-1	519	51.9	94.5	631	1.5	27	22.5	7.56	7.67	14.7	10.62	11.47	22.09
CS-4	544	58.3	183	123	2.6	50	33.33	6.68	2.39	31.1	17.08	17.56	34.64
CS-6	513	46.8	74.2	651	1.6	28	21.54	8.05	6.64	14.3	8.56	11.14	19.7

Table 4: Chemical analysis of some trace elements and ΣREEs and their chemical ratios.

Citation: Heikal MTS, Monsef MA, Goma SR, Mansi M, Top G (2018) Natural Radionuclides Levels and their Geochemical Characteristics of Abu Dabbab Albite Granite Mining Area, Central Nubian Shield of Egypt. J Environ Hazard 1: 108.

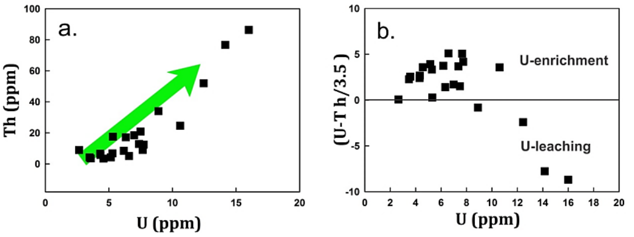

Figure 8 : (a,b) Variation diagrams among U, Th (ppm) relevant to chemical analysis using ICP-MS technique for Abu Dabbab albite granite. Line separating takes place between U-enrichment and U-leaching in Figure 8d, after Boyle, 1982.

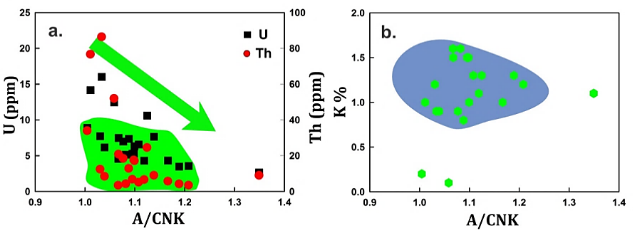

Figure 9: (a,b) A/CNK *vs.* U, Th (ppm) and K% of the studied samples. A/CNK = molar ratio of Al_2O_3/ ($CaO + Na_2O + K_2O$).

In respect of some selected trace elements; Nb, Ta, Zr, Hf, Rb, Sn and Y, ΣLREEs, ΣHREEs, ΣREEs *vs* U, Th and K (Figures 11 and 15), the studied albite granite is characterized by very high contents of Rb and Sn (up to 1050, 3900 ppm, respectively), high contents of Ta, Nb, Zr and Hf (up to 473, 165, 101 and 70 ppm respectively) (Table 4). Whereas ΣREEs have low values (up to 34.64) (Table 4).

Variation diagrams among U and some selected trace elements (Figures 11a-11h) reveal a positive correlation with Ta, Nb, Zr, Hf (Figures 11a, 11b, 11d and 11g) and moderate positive relation with Sn, Y (Figures 11c and 11f), indicating strong magmatic processes (Zr, Hf) followed by post magmatic processes, including Na- metasomatic albitization and mineralization (Ta, Nb, Sn). On the other hand, Zr/U vs. U and Rb vs. U diagrams (Figures 11e and 11h) give rise to decreasing trends. This is attributed to the U ion which is about the same size as the Zr ion, U will substitute for Zr and crystallize in zircon [46], and Rb is commonly included within the crystal structure of potassium feldspar and enriched in the late - phase process [14].

With respect to Th *vs* the same trace elements mentioned above (Figures 11a-11h); the present plots (Figures 12a-12h) confirm the same chemical behaviour of the studied albite rocks as explained in Figures 11a-11h.

On the basis of variation diagrams between K% and Ta, Nb, Sn, Zr, Zr/K%, Y, Hf and Rb (Figures 13a-13h), almost variation diagrams show irregular trends (Figures 13a-13d and 13f-13g). Exceptional two variation diagrams, K% *vs.* Zr/K% & Rb (Figures 13e and 13h) indicate negative and positive correlation respectively.

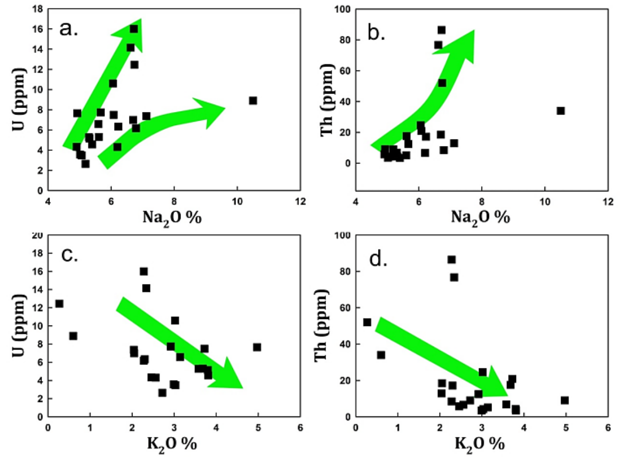

Figure 10: (a-d) Variation diagrams among U & Th (ppm) vs some major elements.

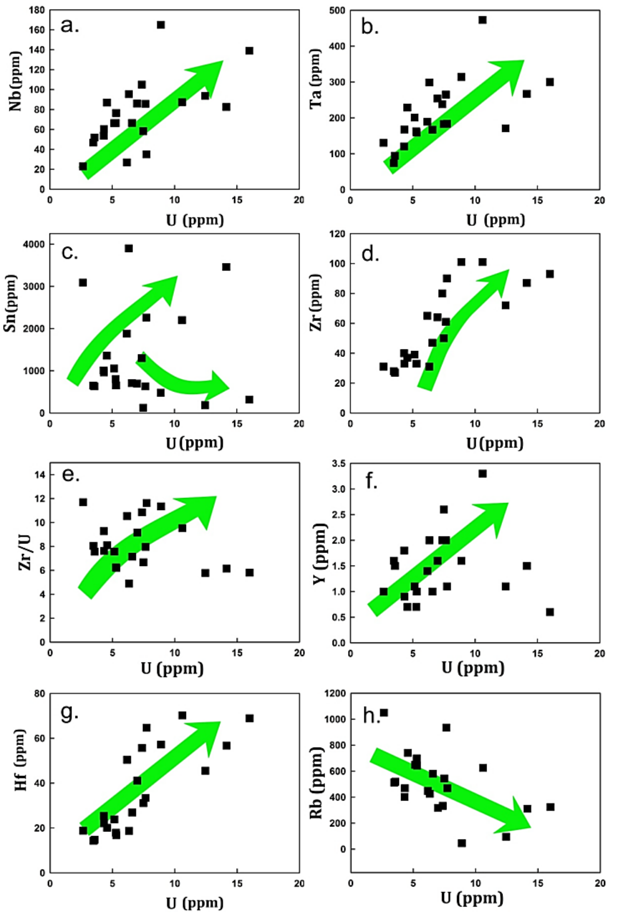

Figure 11: (a-h) Variation diagrams among U (ppm) *vs* some trace elements of the studied samples.

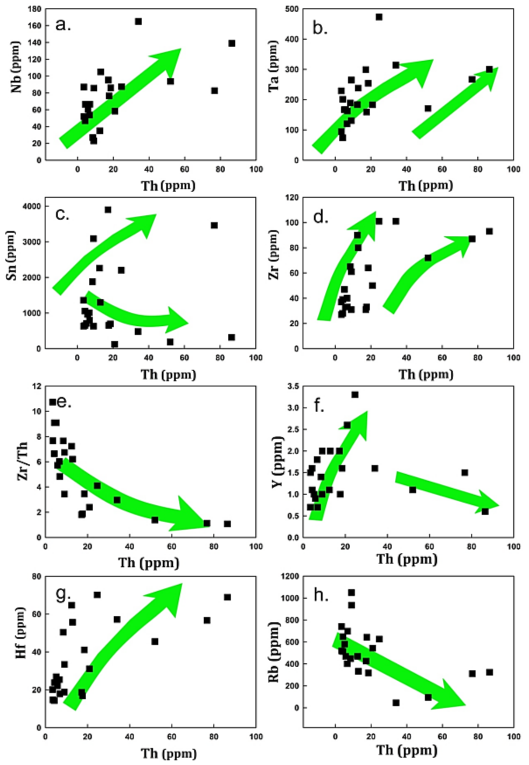

Figure 12: (a-h) Th *vs.* some trace elements of the studied samples.

The irregular trends are due to hydrothermal pervasive alteration (amazonitization) process [32] whereas the strong negative and positive trends (Figures 13e and 123h) are attributed to Zr depletion with respect to K% in which maximum value of Zr (101 ppm, Table 4) meets 0.1 K% (Table 3), whereas Rb occurs as a minor trace element constituent in alkali feldspars.

The results obtained from ICP-MS measurements of U/Th and Th/U ranged from 0.18 to 1.32 with an average of 0.62 and from 0.75 to 5.42 with an average 2.22 ppm respectively (Table 3). The mean values of U/Th are higher than the global ratios 0.3, whereas Th/U is lower than the world average ratio 3.5 for granites [47,32]. Therefore we consider these Th/U ratios as a result of magmatic processes.

The variation diagrams between Th/U and some trace and rare earth elements (Figures 14a-14h), reveal a slight positive correlation for all elements; Nb, Ta, Sn, Zr, Y, Hf, ΣLREEs, ΣHREEs and ΣREEs (Figures 14a-14e & 14g-14l) except Rb that shows moderate negative correlation *vs* Th/U (Figure 14f). This confirms magmatic origin followed by post-magmatic processes had been elucidated for the studied albite granites.

It is well known that, there is a distinct relationship between enrichment or depletion of REEs and their relevant U and Th concentrations [2,5,48]. This is attributed to the presence of REEs and radioactive elements with variable proportions of the accessory minerals in felsic igneous rocks. The variation diagrams among U& Th *vs.* Σ LREEs, Σ HREEs and Σ REES (Figures 15a-15f) reveal a moderate positive correlation indicating a magmatic signature.

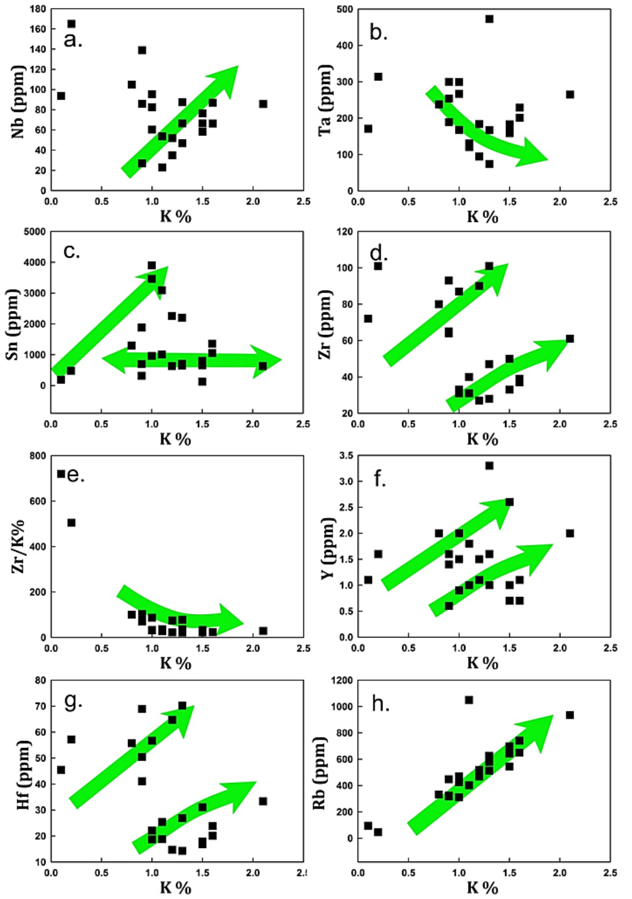

Figure 13: (a-h) Variation diagrams among K% *vs.* some trace elements for the studied samples.

Equilibrium/disequilibrium state (P-& D-factor)

$^{226}Ra/^{238}U$ and $^{238}U/^{226}Ra$ equilibrium (P-factor): The ^{238}U natural radioactive series consists of nuclides with different chemical and physical properties. Their half-lives range from less than 1 s up to trillions of years. On the other hand, the equilibrium factor, which was defined by [49] as P-factor and expressed as the ratio between radio metrically measured equivalent uranium and equivalent radium (eU/eRa).

It was calculated in all studied rock samples giving rise to ratio >1 (Table 2). This reflects the state of disequilibrium, while P-equal unity indicates the state of equilibrium.

In general, granitic rocks are considered to be in radioactive secular equilibrium due to its crystallization age, which is usually above 5 Ma [19]. However, if the rock is fractured or chemically altered, the isotopic system can be seriously affected by the interaction that occurs between the rock and hydrothermal solutions. Therefore, the mobilization of the U radionuclides (^{238}U and ^{226}Ra) occurs more than Th due to faster mobility. In this study, the radioactive secular equilibrium in the ^{238}U series has been examined by assessing the $^{226}Ra/^{238}U$ ratios. The average of all studied surface, adit and core

Citation: Heikal MTS, Monsef MA, Goma SR, Mansi M, Top G (2018) Natural Radionuclides Levels and their Geochemical Characteristics of Abu Dabbab Albite Granite Mining Area, Central Nubian Shield of Egypt. J Environ Hazard 1: 108.

subsurface samples have $^{226}Ra/^{238}U$ ratios; 07, 0.6 and 0.57 respectively, i.e. <1 (Table 2).

According to the fact that the greisenization is very common within the present granite stock, therefore the hydrothermal alteration appears to be severe, so <1 is very normal. In addition, the enrichment in 238U is probably due to its re- redistribution [6,13] as well as re-mobilization in the studied rocks in combination with 226Ra removal, supposing that the geochemical conditions favour a greater mobility of Ra compared to U. This is consistent with published work by [19].

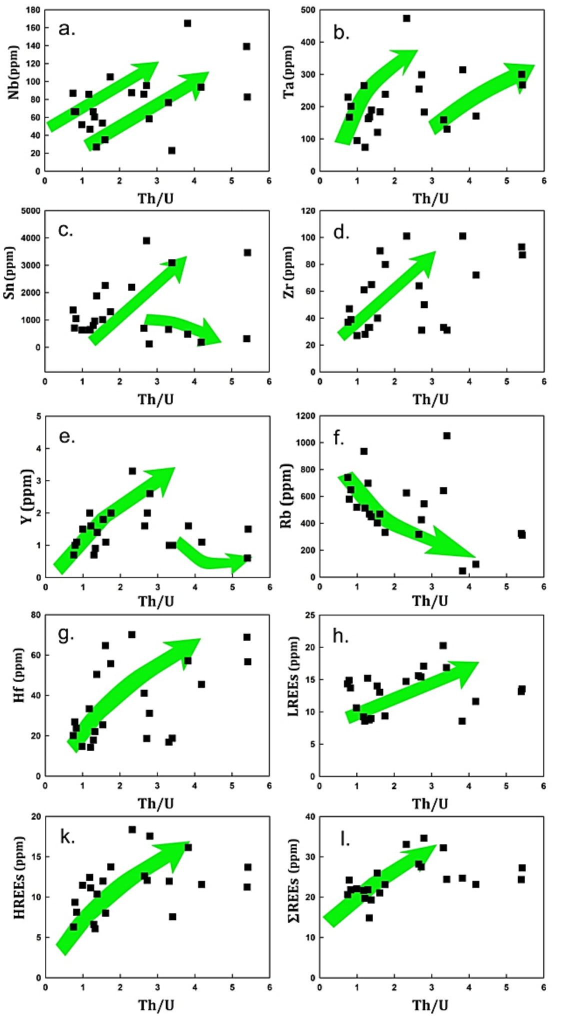

Figure 14: (a-l) Th/U *vs.* some trace elements and rare earth elements (REEs) of the studied samples.

Uc/Ur equilibrium/disequilibrium state (D-factor): Another method for the detection of the equilibrium/disequilibrium states has been introduced by [50], who defined the equilibrium (D factor) state as the ratio between the chemically determined uranium (Uc) and the radiometrically determined (Ur):

ER=Uc /Ur

The equilibrium state is achieved if the equilibrium ratio is in unity; whereas deviation from unity provides disequilibrium state which indicates an addition or removal of uranium. In the present studied rocks, the average Uc is 7.13 (Table 3), whereas the average of Ur is 6.29 (Table 2), thus, the average ratio is about 1.13, i.e. >1 confirming disequilibrium state and recent uranium leaching (addition) of uranium.

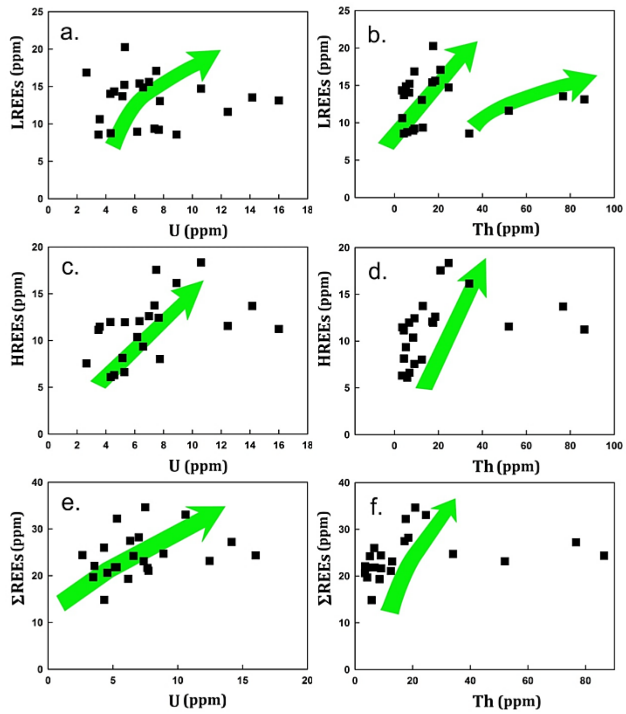

Figure 15: (a-f) Variation diagrams among U, Th *vs.* rare earth elements for the studied samples.

Conclusion

Abu Dabbab rare metal-bearing albite granite (0.4 km^2) represents a unique special felsic rock type forming stock-like intrusion (650-570 Ma). It intruded into the ophiolitic mélange country rocks with sharp contacts. It is located in the northwestern part of Marsa Alam town, central Nubian Shield of Egypt. The studied granitic stock is intersected by two master fault and/or tensional shear zones as well as highly dissected by quartz and amazonite veins. To draw the main characteristic features are relevant to the distribution of radioactivity levels (^{238}U, ^{226}Ra, ^{232}Th and ^{40}K) and their origin for the studied Abu Dabbab rare metals-bearing albite granite, the concluding remarks are as follows:

1. The reconnaissance *in situ* points sample measurements using portable gamma ray RS-230 spectrometer indicate that the high total gamma activity tends to nearby shear zones and quartz-amazonite veins (Table 4).

2. The detailed laboratory radiometric measurements using a gamma ray HPGe detector (Tables 2 and 3) indicate that some samples 40 K activity is very poor while ^{238}U and ^{232}Th is high due to multi-enrichment processes like remobilization and re-distribution processes followed after the magmatic process. The radioactivity level of the

studied radioactivity levels of the studied radionuclides appears to be non-uraniferous granite [44].

3. Some rock slides, a complete replacement of K-feldspar by albite have been ascribed to a mechanism of ions exchange between fluid and feldspar phases [51], the replacement reaction is expressed by [52]:

$KAlSi_3O_8 + Na+ \leftrightarrow NaAlSi_3O_8 + K+$
(microcline) (albite)

4. The detailed chemical analysis of the studied radionuclides and some major, trace and rare earth elements, using ICP-MS & OES techniques, explained the main geochemical correlations of the radioelements together with some selected chemical elements.

5. The obtained chemical data (Tables 3 and 4) of the studied radioactive elements and other selected major and trace elements are consistent with the same conclusions for radioelements origin referred to the radiometric measurements in both field and laboratory techniques. The chemical interpretations given for many variation diagrams of U. Th and K as well as selected major, trace and rare earth elements indicate that the magmatic process followed by Na-metasomatic albitization do occur, and the later process caused redistribution and remobilization of U giving rise to enrichments [53-55].

6. Hydrothermal fluid circulation and greisenization are common along the shear zones of the studied rare metals-bearing albite granite could have changed Eh and pH conditions and helped to oxidization of uranium from tetravalent into a hexavalent state [48]. The converted hexavalent uranium might be leached out of the system and later redistributed along the structurally shear zones due to its high soluble nature.

7. The calculated radioelement concentrations depends on total gamma radioactivity by RS-230 (Table 1) are twice more than those determined by the spectrometric laboratory and chemical analysis method. This result is consistent with published works by [56].

8. The P-& D-factors calculated for the studied radioactive elements indicate that the disequilibrium state is well recognized in the studied albite granite, confirming recent U-leaching.

9. After statistical analyses and data mining, local heterogeneities of the radionuclide distribution were determined, in which the median values of risk indices are lower than the permissible levels leading to safe inhibitancy places for mining workers [1].

References

1. Heikal MTS, Gomaa SR, Abd El, Monsef M, Taha A, et al. (2018) Insight on radiological risk assessment and its statistical evaluations for Abu Dabbab Albite granite mining area, Central Nubian Shield, Egypt. Arab J Nuc Phy Applic 51: 143-167.
2. Mercadier J, Cuney M, Lach P, Boiron MC, Bonhoure J, et al. (2011) Origin of uranium deposits revealed by their rare earth element signature. Terr Nov 23: 264-269.
3. Atwood DA (2012) The rare earth elements: Fundamentals and applications. Joh Wil Son 1: 606.
4. Jha AR (2014) Rare earth materials: Properties and applications. CRC 1: 329.
5. Heikal MThS (2014) REEs and RM-bearing minerals and their economic aspects. LAP LAMBERT 1: 64.
6. Heikal M Th S, Top G (2018) Assessment of radioactivity levels and potential, and radiation hazards health of madsus granites and associated dikes nearby and around Ruwisat Village, South Sinai, Egypt. J Afric Eart Sci 146: 191-208.
7. Pękala M, Kramers JD, Waber, HN (2010) 234U/238Uactivity ratio disequilibrium technique for study in uranium mobility in the Opalinus Clay at Mont Terri, Switzerland. Appl Radiat Isot 68: 984-992.
8. Roger JJW, Adams JAS (1969) Uranium and thorium. In: Wedepohl. Spring 1: 11-13.
9. Smith JR (1984) Uranium mineralogy. In: De Vivo B, Ippolito F, Capaldi G and Simpson PR, Uranium Geochemistry, Mineralogy, Geology, Exploration and Resources. Inst Min Metal 1: 43-88.
10. Finch R, Murakami T (1999) Systematics and paragenesis of uranium minerals. Environment Rev Mineral 38: 91-179.
11. El-Sharkawy A, Heikal MTS, Shreif MI, Badran H (2012) Enviromental Assessment of Gamma levels Radiation in stream sediments around Sharm El Sheikh town,South Sinai,Egypt. J Environ Radioact 112: 76-82.
12. Heikal MTS, El Dousky BT, Ghoneim MF, Sherif MI (2013) Natural radioactivity in basement rocks and stream sediments, Sharm El Sheikh area, South Sinai, Egypt: Radiometric levels and their significant contributions. Arab Journal Geosci. 6: 3229-3239.
13. Heikal MTS, Mahmoud KR, El Sobky T, Top G (2016) Toward assessment the high gamma dose levels and relevant human health impacts from precambrian granites, Na'wah Area, Yemen Republic. Inter J Env Water 5: 1-12.
14. Erkül ST, Ozmen SF, Erkül F, Boztosun I (2016) Comparison between natural radioactivity levels and geochemistry of some granitoids in western Turkey. Turkish J Earth Sci 25: 242-255.
15. El Afifi EM, Shahr El-Din AM, Aglan RFEH, Borai EH, Abo-Aly MM (2017) Baseline evaluation for natural radioactivity level and radiological hazardous parameters associated with processing of high grade Monazite. Regul Toxicol Pharmacol 89: 215-223.
16. Plater AJ, Dugdale, RE, Ivanovich M (1994) Sediment yield determination using uranium-series radionuclides: the case of the wash and Fenland drainage basin. East Eng Geomor 11: 41-56.
17. Pelt E, Chabaux F, Innocent C, Navarre-Sitchler AK, Sak PB, et al. (2008) Uranium thorium chronometry of weathering rinds: rock alteration rate and Paleo-isotopic record of weathering fluids. Earth Planet Sc Lett 276: 98-105.
18. Bourdon B, Bureau S, Andersen MB, Pili E, Hubert A (2009) Weathering rates from top to bottom in a carbonate environment. Chem Geol 258: 275-287.
19. Papadopoulos A, Şafak AS, Koroneos A, Alp ÜA, Kamaci O (2017) Geochemistry of uranium and thorium and natural radioactivity levels of the western Anatolian plutons, Turkey. Miner Petrol 111: 677-691.
20. Langmuir D, Herman JS (1980) The mobility of thorium in natural waters at low temperatures. Geochim Cosmochim Acta 44: 1753-1766.
21. Rosholt J (1982) Mobilization and weathering. In: Ivanovich M, Harmon RS. (Eds.), Uranium Series Disequilibrium: Application to Earth, Marine and Environmental Science. Oxf Sci Pub 1: 167-180.
22. Scott MR (1982) The chemistry of U- and Th-series nuclides in rivers. In: Ivanovich, Application to Earth, Marine and Environmental Science. Oxf Sci Publicat 1: 180-201.
23. Osmond JK, Ivanovich M (1992) Uranium-series mobilization and surface hydrology. Oxf Sci Publicat 1: 259-289.
24. Chabaux F, Riotte J, Dequincey O (2003) U-Th-Ra fractionation during weathering and river transport. Rev Mineralog Geochem 52: 533-576.
25. Mahmoud HA (2017) Phanerozoic Extensional Faulting and Alteration Control on Uranium Mineralization in Trachytes of the Central Eastern Desert of Egypt. J Afric Eart Sci 136: 282-304.
26. Kröner A (1985) Ophiolites and the evolution of tectonic boundaries in the Late Proterozoic Arabian Nubian Shield of NE Africa and Arabia. Precam Res 27: 277-300.
27. Vail JR (1989) Pan-African (Late Precambrian) tectonic terrains and the reconstruction of the Arabian Shield. Geology 13: 839-842.

28. Sabet AH, Chbanenko V, Tsogoev V (1973) Tin-Tungsten and rare metal mineralization in the Central Eastern Desert of Egypt. Geol Surv Egypt Cairo Egypt Ann 3: 53-86.
29. Helba H, Trumbull RB, Morteani G, Khalil SO, Arslan A (1997) Geochemical and petrographic studies of Ta mineralization in the Nuweibi albite granite complex, Eastern Desert, Egypt. Miner Deposits 32: 164-179.
30. Küster D (2009) Granitoid-hosted Ta mineralization in the Arabian-Nubian Shield: ore deposit types, tectono-metallogenetic setting and petrogenetic framework. Ore Geol Rev 35: 68-86.
31. Mohamed AM (2012) Immiscibility between silicate magma and aqueous fluids in Egyptian rare-metal granites: melt and fluid inclusions study. Arab J Geosci 1: 15-25.
32. El Hadek HH, Mohamed MA, Bishara WW, El Habaak GH, Ali KA (2016) Evolution of mineralizing fluids of greisens and fluorite veins, evidence from fluid inclusions. Inter J Geophys Geochem 3: 49-56.
33. Stern RJ, Hedge CE (1985) Geochronologic and isotopic constraints on late Precambrian crustal evolution in the Eastern Desert of Egypt. Am J Sci 285: 97-127.
34. El-Tahawy MS, Higgy RH (1995) Natural radioactivity in different types of bricks fabricated and used in the Cairo region. App Radiat Isotop 46: 1-11.
35. Mantazul IC, Alam MN, Ahmed AKS (1998) Concentration of radionuclides in building and ceramic materials of Bangladesh and evaluation of radiation hazard. J Rad analytic Nuc Chem 231: 117-122.
36. El-Afandy AH, El-Feky MG, Samia T, El Minyawi SM, Salem HA (2016) Distribution of Radioelements and Evaluation of Radiological Hazard effects on Stream Sediments and Cataclastic Rocks of Wadi Abu Rusheid, Southeastern Desert, Egypt. J Geo Eart Sci 4: 56-69.
37. UNSCEAR (2008) Sources of Ionizing Radiation. Unit Nat 1: 1-15.
38. ICRP (2014) Recommendations of the International Commission on Radiological Protection. ICRP 43: 126.
39. Said AF, Salam AM, Hassan SF, Mohamed WS (2010) Assessment of the Environmental Radioactivity Impacts and Health Hazards Indices at Wadi Sahu Area, Sinai, Egypt. Radiat Phy Protect Conf 27: 145-159.
40. Iovine G, Guagliardi I, Brunol C, Greco R, Tallarico A, et al. (2017) Soil-gas radon anomalies in three study areas of central-northern Calabria (southern Italy). Natural Hazards. 91: 193-219.
41. Abdel Meguid AA, Ammar SE, Ibrahim TMM, Ali KG, Shahin HA, et al. (2003) Uranium Potential of Eastern Desert Granites, Egypt. NMA 1: 270.
42. Macfarlane PA, Whittemore DO, Townsend MA, Doventon JH, Hamilton VJ, et al. (1989) The Dakota Aquifer Program Annual Report, FY89. Geolog Surv Open File Rept 1: 90-27.
43. Ong YH, Shallehhuddin BMJ (1988) Promising uranium in the Central Belt Area, Peninsular Malaysia. Geol Explorat Vien 1: 97-107.
44. Clark SP, Peterman ZE, Heier KS (1966) Abundances of U, Th, K in "Hand book of physical constants, Clark, S. P (Ed.)". The Geological Society of America Memoir, 97:521-541.
45. Boyle RW (1982) Geochemical Prospecting for Thorium and Uranium Deposits. Developments in Economic Geology 16, Elsevier, 508 p.
46. Collins GL (1999) Equal time for the origin of granite-a miracle. Reports Nation Cen Sci Educat 19: 20-28.
47. UNSCEAR (1988) United Nations Scientific Committee on the Effects of Atomic Radiation Sources, effects and risks of ionizing radiation.
48. Frimmel HE, Schedel S, Bratz H (2014) Uraninite chemistry as forensic tool for provenance analysis. Applied Geochemistry 48: 104-121.
49. Hussein AH, Abdel Monem AA, Mahdy MA, El-Aassy IE and Dabbour GM (1992) On the genesis of surficial uranium occurrences in west central Sinai, Egypt. Ore Geol Rev7: 1-15.
50. Hansink JD (1976) Equilibrium analyses of sandstone roll-front uranium deposits. Inter Atomic Ener Agency 1: 683-693.
51. Orville RM (1963) Alkali ion exchange between vapor and feldspar phases. American Journal of Science 261, 201-237.
52. Moore DE, Liou JG (1979) Chessboard-twinned alite from Franciscan metaconglomerates of the Diablo Range, California. Americ Mineralog 64: 329-336.
53. Manning DAC (1981) The effect of fluorine on liquid phase relationships in the system qz-Ab-or with excess water at 1 kbar. Contrib Mineral Petrol 76: 257-262.
54. Kyser K, Cuney M (2008) Recent and not-so recent developments in uranium deposits and implications for exploration. Mineralog Assoc Seri 39: 1-14.
55. Cuney M (2010) Evolution of uranium fractionation processes through time: Driving the secular variation of uranium deposit types. Econ Geol 105: 553-569.
56. Gaafar I (2014) Geophysical Mapping, Geochemical Evidence and Mineralogy for Nuweibi Rare Metal Albite Granite, Eastern Desert, Egypt. Open J Geol 4: 108-136.